Y-Dy DOPED AND CO-DOPED TiO$_2$. ENHANCEMENT OF PHOTOCATALYTIC ACTIVITY UNDER VISIBLE LIGHT IRRADIATION

Wannes KALLEL, Soraa BOUATTOUR

University of Sfax-Faculty of Science-Laboratory CI, Sfax, Tunisia, wanneskallel@yahoo.fr

Abstract: Nano-sized Y-Dy doped and co-doped TiO$_2$ particles were synthesized using the sol–gel method and Ti(OBu)$_4$ as TiO$_2$ precursor for sol-gel process. Their structure and optical properties were examined by XRD, Raman and UV-Vis absorption spectroscopies. The XRD and Raman analysis of samples calcined at 400 °C for 2 h showed that all relatively sharp reflections and bands can be attributed to the anatase form of TiO$_2$. Ground state diffuse reflectance absorption studies reveal that both Y and Dy dopant cause deviations of the band gap to higher energies attesting that co-doping the TiO$_2$ with Y and Dy could enhance the photo-catalytic activity by delaying the electron–hole recombination by means of higher energy band gaps. However co-doping TiO$_2$ at a level of 3% (Y, Dy) leads to a significant decrease in the crystallite size of photocatalyst and to a great enhancement of the photodegradation efficiency of methylene blue (MB) under visible light.

Introduction

A great deal of effort has been devoted in recent years to developing heterogeneous photocatalysts with high activities for environmental applications such as air purification, water disinfection, hazardous waste remediation, and water purification (Jimmy et al., 2002a; Antoniadou et al., 2013).

TiO$_2$ is the most widely used photocatalytic material because it acts as photoactive materials for redox/charge-transfer processes due to their electronic structures which are characterized by a filled valence band and an empty conduction band (Fox and Duly, 1996). TiO$_2$ occurs in nature in three crystallographic phases: rutile, anatase and brookite. Anatase is the most commonly employed in photocatalytic applications due to its inherent superior photocatalytic properties (Fujishima et al., 2000; Carp et al., 2004). However, an important drawback of TiO$_2$ for photocatalysis is its band-gap energy (around 3.2 eV) (Chen et al., 2007). In fact, the latter allows the absorption of

only a small fraction of the solar spectrum, corresponding to the UV region ($\lambda < 380$ nm). Alternatively, TiO_2 can be more directly sensitized through the modification of its bulk or surface properties, often through the use of dopants, which is a commonly employed method to improve photocatalytic materials by inhibiting the electron-hole recombination and prolonging the lifetime of charge carriers.

Recently and in view of the growing cases of water contamination, TiO_2-based photocatalysis are considered as a possible remediation process (Joo et al., 2005) since it can induce the oxidation of organic pollutants (Zhu et al., 2005) and their transformation to CO_2. This photodecomposition process usually involves one or more radicals or intermediate species, such as $^\bullet OH$, $O_2^{-\bullet}$, H_2O_2 (Wang et al., 2012). In aqueous media, the hole typically reacts with adsorbed H_2O to produce hydroxyl radical ($^\bullet OH$), a powerful oxidant (Jiang et al., 2013). However, the photoexcited electron generates with O_2 the reactive oxygen species $O_2^{-\bullet}$. They are responsible for the destruction of problematic pollutants (Zheng et al., 2014).

On the other hand, the degrees of aggregation of catalyst nanoparticles and dopant homogeneity have to be carefully controlled in such studies (Jimmy et al., 2002b; Li et al., 2005, Fujishima et al., 2008). Consequently, the manipulation of nanocrystalline powders is essential to optimize photocatalytic efficiency. Indeed, with the decrease of particle size of photocatalyst, the photocatalytic activity can increase dramatically.

Rare earth elements (REE) ions are well known for their ability to form complexes with various Lewis bases in the interaction of these functional groups with the f-orbital (Xie and Yuan, 2003; Yuan et al., 2005). The use of the REE ions such Ln = Eu, Pr, La, Pr, Nd (Parida and Sahu, 2008), as dopants for TiO_2 crystalline can lead to the incorporation of atoms/ions of these elements into TiO_2 crystalline matrices, or to a surface modification. This can provide a potential means to inhibit the combination of photo electron-hole pairs, enlarges the light adsorption of the semiconductor and therefore enhances the visible light photocatalytic activity. In this context, Reszczynska et al. (2015) shows that the dopant nature (Er^{3+}, Yb^{3+} or Er^{3+}/Yb^{3+} ions) and their relative amount affect the structural, optical and luminescence properties of TiO_2, and their relation with the photocatalytic performance under visible light. Moreover, a recent study performed on TiO_2 doped with Er^{3+}, Yb^{3+} and Er^{3+}/Yb^{3+} revealed that a phenol aqueous solutions was successfully degraded under visible light ($\lambda > 450$ nm) using Er/Yb-TiO_2. DRS results showed that when small level of dopant was chosen optical absorption edge was shifted to the red direction due to the charge transfer transition between TiO_2 and RE^{3+} intra - 4f electrons (An-Wu et al., 2003). Lin and Yu (1998) found that the photo catalytic activities of La_2O_3 or Y_2O_3 doped anatase TiO_2 were much better than pure TiO_2, but CeO_2 doped TiO_2 was worse. These results correlated well with those obtained by Parida and Sahu (2008). However, by comparison to pure TiO_2, using (La_2O_3, Y_2O_3 and CeO_2) doped TiO_2 results in a better photocatalytic performance (Choi et al., 1994).

Stengl et al. (2009) have also used REE (La, Ce, Pr, Nd, Sm, Eu, Dy, Gd) for doping titania, the best photocatalytic properties in visible light have been observed for samples doped with Nd^{3+} ions (k = 0.0272 min^{-1} for UV and 0.0143 min^{-1} for visible light). However the much important red shift was identified for the sample doped with Eu^{3+} ions.

In this paper, we report a detailed investigation into co-doping varying amounts of yttrium and dysprosium into TiO$_2$ powders aiming at an understanding on their effects on the structural orderliness, nanocrystallinity and photocatalytic properties of TiO$_2$ nanoparticles. The photocatalytic properties were investigated by employing the photodegradation of three dyes in aqueous phase as a model pollutant.

Experimental methods

Powder preparation

In this work, the preparation of the sample was conducted using sol–gel process. The experimental process involves two steps. The first, called pregelation, in which the alkoxides are hydrolyzed and self-condensed to form three dimensional networks until the ensuing oligomers are no longer soluble and gelation occurs. The second step is the post gelation which initiates after the gelation point and includes all the phenomena that occur during the drying and calcinations process.

Doped and co-doped samples were prepared using the following materials: YCl$_3$ · 6H$_2$O, Ti(OBu)$_4$ and Dy$_2$O$_3$ as precursors (all of them from Aldrich) where X = 1, 2 and 3 is the atomic ratio n$_{(Y)}$/(n$_{Ti}$) in Y doped samples and (n$_{Dy}$)/(n$_{Ti}$) in Dy doped ones.

Dy$_2$O$_3$ was first dissolved in diluted HNO$_3$ with heating, resulting in the formation of a pale colorless stock solution of Dy(NO$_3$)$_3$. It was added to YCl$_3$ · 6H$_2$O dissolved in acetic acid, which functioning as solvent and hydrolysis catalyst. To this mixture, a solution of Ti(OBu)$_4$ was added progressively and kept under magnetic stirring at 80°C temperature until gelation occurs. The final product was dried at 100°C for 24 h and stored at room temperature for use as starting material in this study. This procedure gives rise mesoporous solids, which are initially amorphous and crystallize upon further heating above 400°C for two hours.

Experimental techniques

Scanning electron microscopy (SEM) studies were performed using a Philips XL30 CP microscope equipped with EDX (energy dispersive X-ray), Robinson, SE (secondary electron) and BSE (back-scattered electron) detectors. The sample was placed on an adhesive C slice and coated with Au-Pd alloy 10 nm thick layer.

The XRD patterns were performed using a Seimens D5000 X-ray diffractometer. The powder X-ray diffraction data for the powders were collected at ambient temperature over the range 10 < 2θ < 56° by step scanning, using 2θ increments of

0.02° to determine the crystallographic phases. The crystallite size was determined from the broadening of corresponding X-ray spectral peaks by Scherrer formula (Qinghong et al., 2000):

$$L = \frac{K\lambda}{\beta\cos\theta} \tag{1}$$

where L is the crystallite size, λ is the wavelength of the X-ray radiation (CuK_α = 0.15418 nm), K is the usually taken as 0.89, and β is the line width at half-maximum height. This is the generally an accepted method to estimate the mean crystallite size of nanoparticle.

Micro-Raman system was assembled in our laboratory and uses an excitation wavelength of 532 nm from a CW laser (Single mode Cobolt Sambalaser, 300 mW), coupled by a 200 μm optical fibre to the spectrograph (Headwall, model 532). The Raman probe of our set-up is a Superhead 532 from H-JY. The CCD detectors from Andor, (modelNewton, 1600 pixels), Peltiercooled, works at –60°C, 532 nm Edge, Notch and line filters are from Semrock were applied. The system resolution is 2 cm^{-1} with a 50×Olympus long working distance objective (Bouattour et al., 2013).

Ground-state absorption studies were performed using all powdered samples, by means of an OLIS14-VIS-NIR spectroscopy operating system with diffuse reflectance. The reflectance, R, from each sample was obtained by scanning the excitation monochromator from 240 to 840 nm, and the remission function, $F(R)$, was calculated using the Kubelka-Munk equation for optically thick samples (those where no further increase of the sample thickness can change the experimentally determined R). The remission function, according to Ferreira et al. (1998) is:

$$F(R) = \frac{1-R^2}{2R} . \tag{2}$$

Photocatalytic activity measurements

The visible photocatalytic activity of the prepared Y, Dy doped and co-doped TiO_2 nanoparticles was investigated by monitoring the time change of residual concentration of aqueous solution of three different dyes: methylene blue (Color Index (CI): 52015; Basic Blue 9), methyl red (CI: 13020; Acid Red 2) and methyl orange (CI: 13025; Acid Orange 52) used as pollutants models (Fig. 1).

In each of the experiments, powdered doped titanium dioxide was added as a photocatalyst to 50 cm^3 of aqueous dye solution (C = 10^{-4} mol/dm^3) and shaken vigorously to form a homogenous mixture. The mixture was sonicated (bath sonicator) before irradiation for 10 min to obtain highly dispersed catalysts. Before irradiation, solutions were maintained in the dark for 1 h to promote the dye adsorption onto the photocatalyst surface. The aqueous suspension was kept under magnetic stirring during the entire reaction period to maintain the suspension homogeneity. At constant time intervals, 2 cm^3 aliquots were sampled, immediately centrifuged at 24 000 rpm for 15 min to remove the TiO_2 particles, and then analyzed on a Cecil UV-Vis

spectrophotometer. The UV absorbance of the solutes was measured at their corresponding λ_{max}. Calibration curves were previously established for each solute studied here. A 54 W Halogen lamp was used as visible light source.
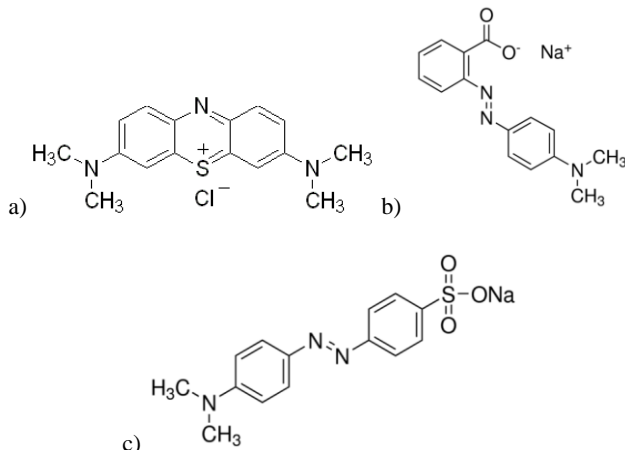

Fig. 1. Molecular structure of (a) methylene blue (b) methyl red and (c) methyl orange

Results and discussion

SEM analysis

SEM observations have been carried out for 3% (Y, Dy) co-doped TiO₂ sample calcined at 400°C. As shown in Fig. 2, the EDX analysis confirmed the presence of all the desired elements even those used at a small level: O, Ti, Y and Dy.
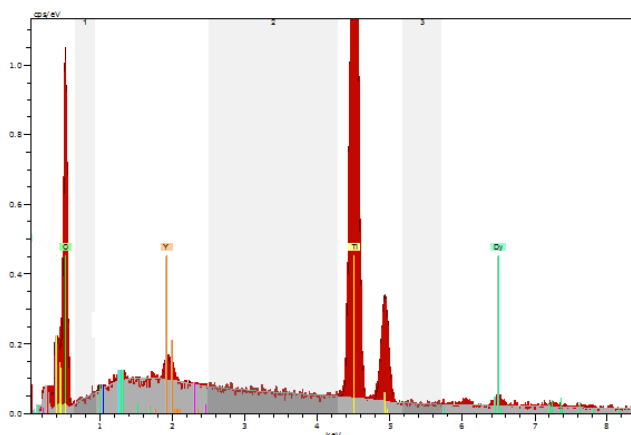

Fig. 2. Energy dispersive X-ray spectra of 3% (Y, Dy) co-doped TiO₂, calcined at 400°C

XRD characterization

XRD was used to investigate the crystallographic form of the as-prepared samples. The XRD patterns of the undoped, doped and co-doped titania after calcinations, at 400°C, are superimposed in Fig. 3. Careful analysis revealed that all relatively sharp reflections can be indexed using the anatase tetragonal structure ($I4_1/amd$) of TiO_2 with a decrease of the crystallinity of powders in the presence of Y or/and Dy as dopants. No peak due to rutile or other titania phase can be detected in all samples. Moreover, Fig. 3 reveals that the XRD reflections of pure, doped and co-doped TiO_2 have the same positions by and large, suggesting that Dy^{3+} and Y^{3+} did not enter TiO_2 crystal lattice to substitute for Ti^{4+}. Additionally, the widening of the reflections can be due to a systematic decrease in grain size and probably structural cristallinity after doping. The average size of crystallites determined by Sherrer formula of pure TiO_2, Y doped, Dy doped, 1% (Y, Dy) co-doped and 3% (Y, Dy) co-doped, calcined at 400°C, is found to be 25, 11, 10, 12 and 6 nm, respectively, demonstrating that doping and co-doping TiO_2 with Y or/and Dy inhibit the growth of TiO_2 particles (Table 1).

Table 1. Crystallite size of the Y-Dy doped and co-doped samples

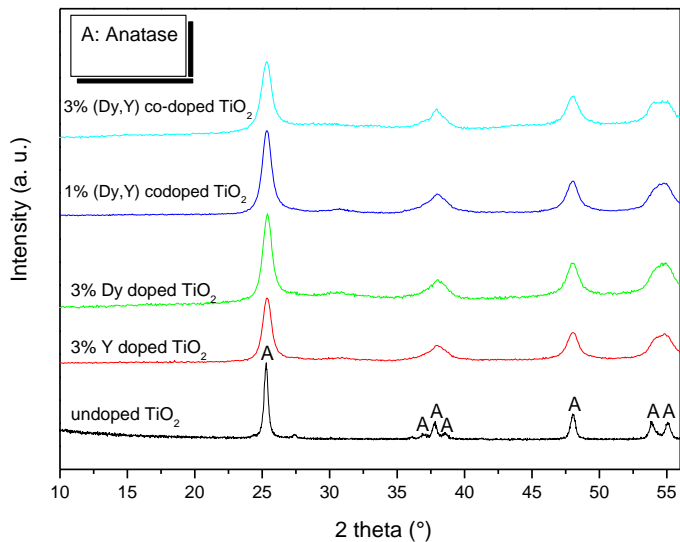| Samples	Undoped TiO_2	3% Y	3% Dy	3% (Dy,Y)	1% (Dy,Y)
Crystallite size (nm)	25	11	10	6	12

Fig. 3. XRD patterns of undoped, 3% Y doped TiO_2, 3% Dy doped TiO_2, 1% (Y, Dy) co-doped TiO_2 and 3% (Y, Dy) co-doped TiO_2 calcined at 400 °C

Ionic radius and calcinations temperature are two important conditions, which strongly influence the ability of the dopant to enter into the TiO_2 crystal lattice to form

stable solid solution. If the ionic radius of the doping ion is much larger, the substitution process can be suppressed (Jun and Jimmy, 1998). The relatively huge difference between the Ti^{4+} (0.064 nm) radius and, Y^{3+} (0.095 nm) and Dy^{3+} (0.175 nm), rationalize that such substitution with Y^{3+} and Dy^{3+} could no to occur, Y^{3+} and Dy^{3+} did not enter TiO₂ crystal lattice to substitute Ti^{4+}. Y^{3+} and Dy^{3+} dopants are adsorbed at the surface of the TiO₂ particles and justify the decreasing of anatase grain size. Thus one can conclude that dopants adsorbed at the particle surface result in a repulsive interaction between positive charge ions (Y^{3+} and Dy^{3+}), prevent the coalescence of nanocrystallites and thereby inhibit their growth. These results corroborate with those obtained by Stengl et al. (2009). They explain the decrease in particle size by the presence of RE-O-Ti in the doped samples, which inhibits the growth of crystal grains.

Raman studies

Raman analysis was applied on undoped TiO₂ and Y-, Dy-doped or co-doped TiO₂ samples as additional tool to probe the phase formation of catalyst. Raman spectra of the samples calcined at 400°C are presented in Fig. 4. It is known that the Raman spectrum of TiO₂ anatase displays five main characteristic bands at wave numbers of 145, 199, 399, 516 and 639 cm⁻¹ (Table 2). These values corroborates with those cited in bibliographies (Ohsaka et al., 1978; Pfalaras et al., 2000). No impression of secondary phase related Raman modes are seen in the doped and co-doped samples spectra. This is in agreement with the XRD results. In this work the E_g mode, mainly attributed to symmetric bending vibration appears at 147 cm⁻¹ for the undoped TiO₂, whereas it shifted to 155 cm⁻¹ for 1% (Y, Dy) co-doped TiO₂ sample (Table 2). It is also broader than the one observed in the undoped spectra. In earlier works it has been reported that doping TiO₂ by some transition and other rare earth generates oxygen vacancies and results in a shift the E_g band to higher wavenumber (Sumsmita et al., 2014).

Table 2. Raman bands of anatase form for undoped, Y or/and Dy doped TiO₂ samples

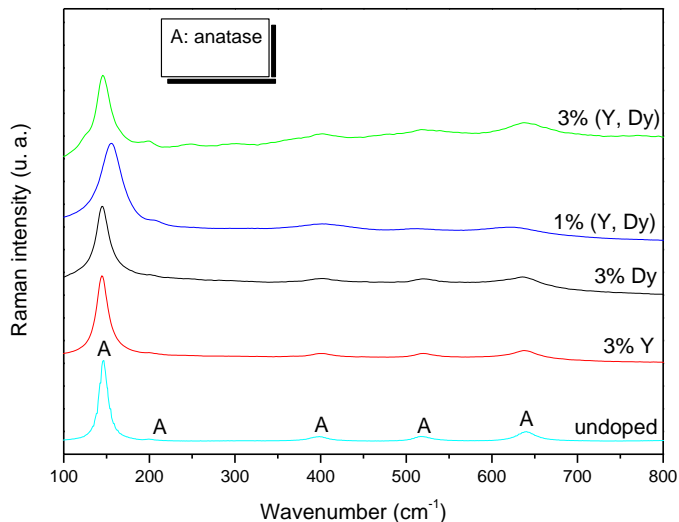| Samples	Bands E_g	E_g	B_{1g}	$A_{1g} + B_{1g}$	E_g
undoped	147	207	397	519	640
3% Y	145	203	400	519	638
3% Dy	145	203	400	519	635
1% (Y, Dy)	155	206	403	514	628
3% (Y, Dy)	145	198	403	519	638

Fig. 4. Raman spectra of undoped, Y or/ and Dy doped TiO_2 samples annealed at 400 °C

Ground state diffuse reflectance spectra

The corresponding UV-Vis diffuse reflectance spectra of the pure TiO_2, and Y-, Dy-doped or co-doped TiO_2 samples are superimposed in Fig. 5. The reflectance edge shifts toward shorter wavelengths for Y-, Dy-doped or co-doped TiO_2 powders compared to undoped spectra. This indicates an increase in the band gap energy of TiO_2 (Table 3).
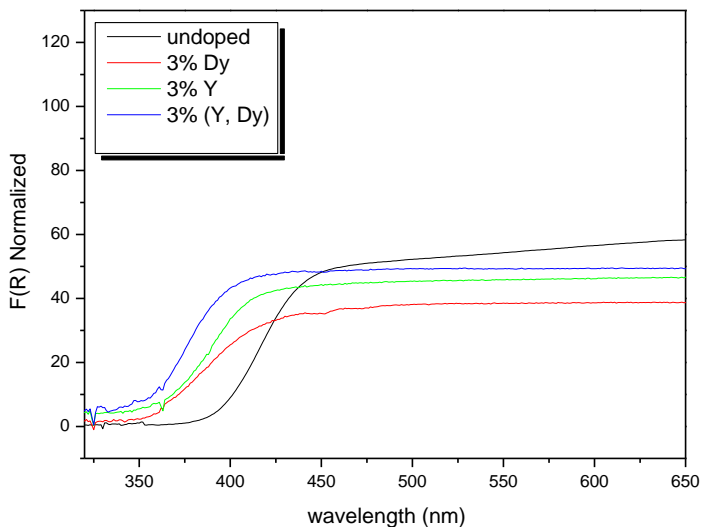

Fig. 5. Ground-state diffuse reflectance absorption spectra of powders of undoped, doped and co-doped TiO_2 with Y and Dy

Table 3. Energy gaps, λ_{abs} (nm) of undoped, Y and/or Dy doped TiO_2

Samples	λ_{abs} (nm)	E_g (eV)
Undoped TiO_2	373	3.31
3% (Dy, Y)	348	3.55
3% Dy	355	3.48
3% Y	359	3.44

As the size of the TiO_2 nanoparticles is varied, the energy levels of the valence and conduction bands are shifted, with an increase of the energy gap between the valence and conduction bands. In this study a value of TiO_2 energy gap of 3.31 eV was obtained for undoped TiO_2 nanoparticles, while a common reported value for this energy gap is 3.2 eV (Xiangxin et al., 2012). These results are compatible with the very small nanoparticles evidenced by XRD analysis and Sherrer formula, leading to strong quantum confinement effects responsible for the high energy gaps (Soraa et al., 2010). Ground state diffuse reflectance absorption studies for the nanopowders show that both the Y and Dy dopant cause deviations of the band gap to higher energies (Table 3) revealing that doping the TiO_2 with Y and Dy could enhance the photo-catalytic activity of the sample, while delaying the electron-hole recombination by means of higher energy band gaps.

Photocatalytic degradation

To investigate the photocatalytic efficiency of the Y-Dy doped and co-doped TiO_2, three dye compounds were used as pollutants models. Given the serious health risks associated with the presence of these compounds in the environment, predominantly in the aqueous phase, we think that their use is interesting to study.

Although the photodegradation process using TiO_2 as catalyst, has been very effective in the decomposition and mineralization of organic pollutant in water under UV illumination, its efficacy under visible light irradiation is still an interesting subject of research studies, posing the need for development of efficient visible-light-active TiO_2 photocatalysis for pollutant abatement. In this context, the photocatalytic activity of Y-Dy doped and co-doped TiO_2 was investigated by monitoring the time change of residual concentration ratios of aqueous solution of organic model compounds. Prior to irradiation, the set-up was stored in the dark for 1 h to discard any possible change in the solute concentration resulting from the adsorption process. The residual concentration of pollutant was then followed by UV-Vis spectroscopy by measuring the absorbance at λ_{max}.

Figure 6 shows the evolution of MB concentration in the absence and in the presence of Y-Dy doped and co-doped TiO_2 powders as a function of irradiation time. It is clear that the MB concentration decreases as the photocatalytic reaction proceeds, since there is a linear relationship between the concentration and the absorption of these compounds according to the Lambert-Beer Equation. As shown in Fig. 6, MB

cannot be degraded in the absence of catalyst. Additionally, in presence of undoped TiO_2, 3% Y, 3% Dy and 1% (Y, Dy) co-doped TiO_2, 96% , 95%, 85% and 90% of MB remained in the solution after 6h of light exposure, attesting the low photocatalytic activity of these catalysts under visible-light excitation. However, increasing the dopants concentration (Y, Dy) at a level of 2% and 3% leads to an important decrease of the residual concentration of MB which attained 50% and 6% respectively. According to the XRD results, TiO_2 exhibits an anatase structure in all the samples calcined at 400°C. These rules out the possibility that the difference in photocatalytic reactivity of the doped and co-doped powders, is caused by the crystalline phase of TiO_2. The high photocatalytic performance of 3% (Y, Dy) co-doped sample is probably due to the particle size which is very small in this case. In fact, small size of catalyst particle favors the increase in the surface-to-volume ratio and the scavenging action of photogenerated electrons by Y^{3+} and Dy^{3+} ions. This could prevent the recombination of photogenerated electron-hole pairs and increase their lifetime, so that charges can take part in photocatalytic processes (Hyun et al., 2012).
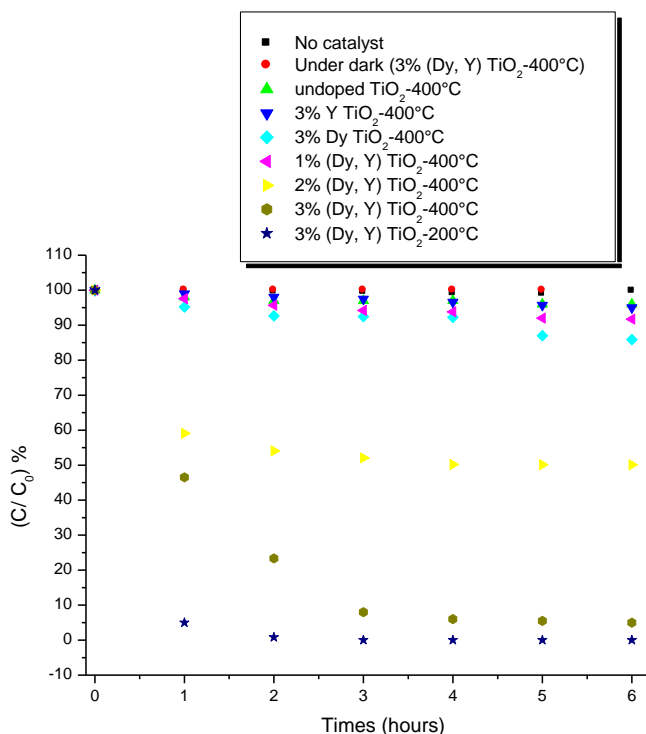

Fig. 6. Evolution of residual concentration of organic solute MB vs time
in the presence of TiO_2 doped and co-doped with Y-Dy under visible irradiation

However, a careful analysis of this figure reveals a quasi total disappearance of MB dye in the presence of 3% (Y, Dy) co-doped TiO$_2$ sample calcined at 200°C, after 1 h of light exposure. The kinetic reaction (irradiation) time of MB is fast. A plausible explanation of this behavior could be that the adsorbed MB inhibits the activation of the photocatalyst. However, the adsorption of MB influences the kinetics of the photocatalytic reaction (Stengl and Kralova, 2011).

On the other hand, a careful analysis of Fig. 7 reveals that the better photodegradation performance is observed for MB compared to Methyl orange and Methyl red, in presence of TiO$_2$ co-doped with 3% (Y, Dy). In fact, after 6 h exposure, the residual concentration ratio attains about 80, 82 and 6% for Methyl orange Methyl red and MB, respectively. The degradation rate of two last organic solutes, using 3% (Y, Dy) co-doped TiO$_2$ powder as photocatalyst, is quite low compared the residual concentration ratio attains for MB. We explain these results by the fact that, the conversion profile is dependent on the structure of the organic compound.
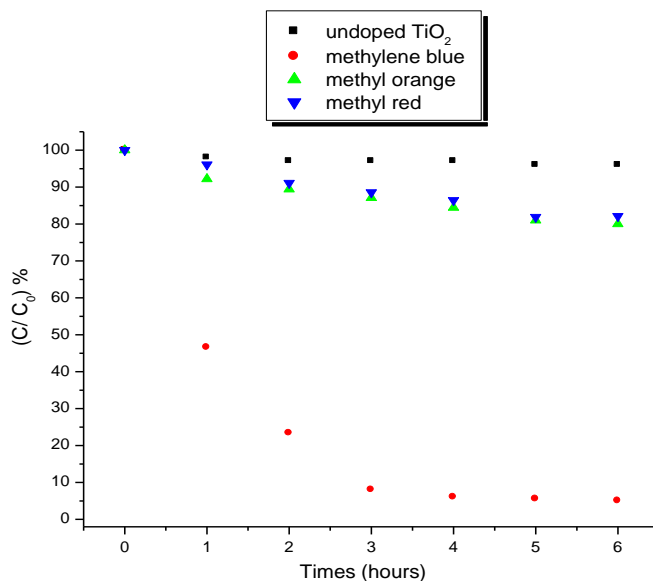
Fig. 7. Evolution of residual concentration of organic solute vs time
in the presence of TiO$_2$ co-doped with 3%(Y, Dy) under visible irradiation

Kinetics of the degradation reaction of aqueous solution of aqueous suspensions of MB pollutant was also investigated. Indeed, the photodegradation results of photocatalyst obey pseudo-first-order kinetics over the time period investigated and the slope equals the apparent degradation rate constant (K_{app}) is an agreement with the generally observed Langmuir-Hinshelwood mechanism. It basically relates the degradation rate and reactant concentration C, in water at time t. When the adsorption

is relatively weak and/or the reactant concentration is low, the system can simplified to a pseudo- first-order kinetics with an apparent first-order rate constant:

$$Ln\left(\frac{C}{C_0}\right) = -K_{app} \cdot t \qquad (3)$$

where C_0 denotes the initial concentration.

For all catalysis, plotting $\ln(C/C_0)$ versus reaction time t yields a straight line, and the slope is the apparent rate constant. Table 4 shows the apparent rate constants K_{app} and regression coefficients R^2 for the photodegradation of MB in the presence of undoped, (Y, Dy) doped and co-doped TiO_2 catalysts. From the data reported in Table 4, the trend in the value of K_{app} is in line with the enhancement in the photocatalytic activity.

Kinetics of MB degradation, in the presence of 3% (Y, Dy) co-doped TiO_2 catalyst, leads to a K_{app} value of 0.492 h^{-1}. This value is very high compared to those observed for the others catalysts attesting the fast MB decolorization in presence of this catalyst. The degradation rate increased with the increasing level of (Y, Dy) co-doping and demonstrating that an appropriate level of this co-doping can greatly enhance the photocatalytic activity of TiO_2 powders.

Table 4. Apparent first-order rate constant K_{app} and correlation coefficient R^2 for photodegradation of M.B. by undoped, doped and co-doped TiO_2 under visible light excitation

Catalysis	$K_{app} \cdot 10^3$ (h^{-1})	R^2
TiO_2	7	0.97
3% Y	14	0.98
3% Dy	24	0.98
1% (Y, Dy)	21	0.97
2% (Y, Dy)	88	0.98
3% (Y, Dy)	492	0.97

However, if the enhancement of the UV photocatalytic activity is well established, as attested by the huge number of published literature and reviews (Kralchevska et al., 2012; Viswanathan and Krishanmurthy, 2012), the origin of the visible-light responses is still a matter of debate. It is well-known that, for effective degradation, the organic substance should be preconcentrated on the surface of the semiconductor particles to effectively utilize the photoexcited charge (Ferreira et al., 1998), in this case, according to the value of energy gap determined by ground state diffuse reflectance spectra. We can consider that the dye is excited in a first time from the ground state to the excited state by the action of the visible light photon. As the energy level of the excited MB and the conduction band (CB) position of catalyst are satisfied overlap, electrons can transfer from the excited dye to the CB of the catalyst. The charge carriers either recombine with the bulk of the TiO_2 material or migrate to the particle

surface where the electron reacts with adsorbed O$_2$, to produce active oxygen radicals, while the holes are scavenged by surface hydroxyl groups to generate strong oxidizing hydroxyl radicals (OH), which can promote the oxidation of organic compound.

On the other hand the presence Y and Dy species adsorbed at the surface of TiO$_2$ samples could improve the degradation efficiency by modifying the surface properties of catalysts.

Repeated use of photocatalyst

The aptitude of photocatalyst to be reused is one of the most important parameters which determine, from an economical point of view, the potential exploitation of a material in practical systems for water treatment. To examine the repeatability of the photoacatalytic activity, the 3% (Y, Dy) co-doped TiO$_2$ sample, calcined at 400°C, was used in three consecutive photodegradation cycles during 6 h of visible light irradiation. The residual concentration was measured after each cycle. After each decomposition reaction, the TiO$_2$ powder was separated and used again in the same conditions. It can be seen from Fig. 8 that the photocatalytic efficiency decreases after three degradation cycles of the tested for MB compounds. It is worthy of note that the reused powder was used without washing or any purification treatment. The residual concentration attained 6, 19 and 37% after three degradation cycles. This result may be explained by the formation of by-products and their accumulation on the active surface sites of the photocatalyst thus making the active site on the surface less available.

Thus, it is clearly shown that 3% (Y, Dy) co-doped TiO$_2$ nanoparticles prepared by sol-gel process according to the method above described displayed higher photocatalytic activity under visible light excitation.
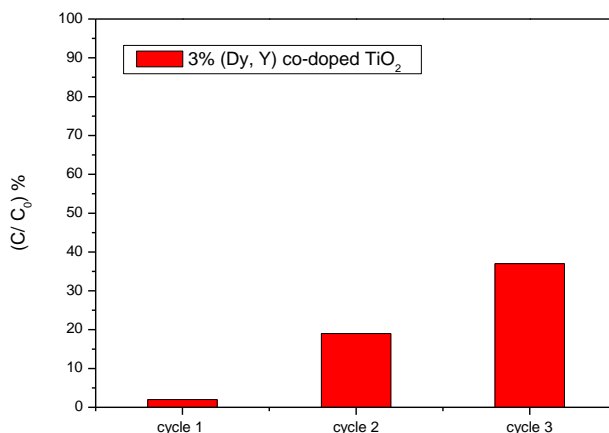

Fig. 8. Evolution of residual concentration of MB vs. time after 6 h
in presence of 3% (Y, Dy) co-doped TiO$_2$ under visible light excitation

Conclusion

Nano-sized Y-Dy doped and co-doped TiO_2 particles were successfully synthesized using the sol-gel method and $Ti(OBu)_4$ as TiO_2 precursor. Their structure and physical properties were examined by XRD, Raman and UV-Vis absorption spectroscopies.

XRD analysis revealed that the anatase particles size decreases with the introduction of dopants. Y^{3+} and Dy^{3+} dopants adsorbed at the particle surface result in a repulsive interaction between positive charge ions which prevent the coalescence of nanocrystallites and thereby inhibits their growth.

Ground state diffuse reflectance absorption studies reveal that dopants cause deviations of the band gap to higher energies attesting that co-doping the TiO_2 with Y and Dy could delay the recombination.

A great enhancement of the visible photodegradation efficiency of MB with the incorporation of Y, Dy dopants simultaneously at a level of 3% was evidenced which reflect the benefic effect of the new surface properties of nanoparticles.

References

ANTONIADOU M., VAIANO V., SANNINO D., LIANOS P., 2013, *Photocatalytic oxidation of ethanol using undoped and Ru-doped titania: Acetaldehyde, hydrogen or electricity generation.* Chem Eng J, 224, 144-148.

AN-WU X., YUE PING F., LI-PING Y., HAN-QIN L., 2003, *A simple method to synthesize Dy(OH)₃ and Dy₂O₃ nanotubes,* J Am Chem Soc, 125, 1494-1495.

BOUATTOUR S., FERREIRA D.P., HAMDI A., FERREIRA L.F.V., DO REGO A.M.B., 2013, *Spectroscopic studies of mixed pyrochlore-oxide(Y/Gd)₂Ti₂O₇ samples prepared via sol–gel and solid-state methodologies and calcined at different temperatures.* Mater Chem Phys, 138, 507-513.

CARP O., HUISMAN C. L., RELLER A., 2004, *Photoinduced reactivity of titanium dioxide*. Prog Solid State Chem. 32, 33-177.

CHEN D., JIANG Z., GENG J., WANG Q., YANG D., 2007, *Carbon and nitrogen co-doped TiO₂ with enhanced visible-light photocatalytic activity.* Ind Eng Chem Res, 46, 2741-2746.

CHOI W., TERMIN A., HOFFMANN M.R., 1994, *The role of metal ion dopants in quantum-sized TiO₂: Correlation between photoreactivity and charge carrier recombination dynamics.* J Phys Chem 98, 13669-13679.

FERREIRA L.F.V., CABRAL P.V., ALMEIDA P., OLIVEIRA A.S., REIS M.J., DO REGO A.M.B., 1998, *Ultraviolet/visible absorption, luminescence and X-ray photoelectron spectroscopic studies of arhodamine dye covalently bound to microcrystalline cellulose.* Macromol, 31, 3936-3944.

FOX M.A., DULY M.T., 1996, *Acceleration of secondary dark reactions of intermediates derived from adsorbed dyes on irradiated TiO₂ powders.* J Photochem Photobiol A Chem, 98, 91-101.

FUJISHIMA A., RAO T.N., TRYK, D.A.J., 2000, *Titanium dioxide photocatalysis.* Photochem Photobiol C, 1, 1-21.

FUJISHIMA A., ZHANG X., TRYK D.A., 2008, *TiO₂ photocatalysis and related surface phenomena.* Surf Sci Rep, 63, 515-582.

HYUN-S. J., HO-B. L., KEUN-H. C., MOO-Y. H., MAAYSA M., SO-H. C., JONG-K. P., 2012, *Nitrogen-doped TiO₂ nanopowders prepared by chemical vapor synthesis: band structure and photocatalytic activity under visible light.* Res Chem Intermed, 38, 1171-1180.

JIANG W., JOENS J.A., DIONYSIOU D.D., O'SHEA K.E., 2013, *Optimization of photocatalytic performance of TiO₂ coated glass microspheres using response surface methodology and the application for degradation of dimethyl phthalate.* J Photochem Photobiol A 262, 7-13.

JIMMY C.Y., JIAGUO Y., JINCAI Z., 2002a, *Enhanced photocatalytic activity of mesoporous and ordinary TiO₂ thin films by sulfuric acid treatment.* Appl Catal B Environ, 36, 31-43.

JIMMY C.Y., LZIHI Z., JIAGUO Y., 2002b, *Rapid synthesis of mesoporous TiO₂ with high photocatalytic activity by ultrasound-induced agglomeration.* New J Chem, 26, 416-420.

JOO J., KWON S.G., YU T., CHO M., LEE J., YOON J., HYEON T., 2005, *Large-scale synthesis of TiO₂ nanorods via nonhydrolytic sol–gel ester elimination reaction and their application to photocatalytic inactivation of E. coli.* J Phys Chem B 109, 15297-15302.

JUN L., JIMMY C.Y., 1998, *An investigation on photocatalytic activities of mixed TiO₂-rare earth oxides for the oxidation of acetone in air.* J Photochem Photobiol A Chem, 116, 63-67.

KRALCHEVSKA R., MILANOVA M., TISLER T., PINTAR A., TYULIEV G., TODOROVSKY D., 2012, *Photocatalytic degradation of the herbicide iodosulfuron by neodymium or nitrogen doped TiO₂.* Mater Chem Phys, 133, 1116-1126.

LI D., OHASHI N., HISHITA S., KOLODIAZHNYI T., HANEDA H., 2005, *Origin of visible-light-driven photocatalysis: A comparative study on N/F-doped and N–F-codoped TiO₂ powders by means of experimental characterizations and theoretical calculations.* J Solid State Chem, 178, 3293-3302.

LIN J., YU J.C., 1998, *Investigation on photo catalytic activities of mixed TiO₂-rare earth oxides for the oxidation of acetone in air.* J Photochem Photobiol A Chem, 116(1), 63-67.

OHSAKA T., IZUMI F., FUJIKI Y., 1978, *Raman spectrum of anatase TiO₂.* J Raman Spectr, 7, 321-324.

PARIDA K. M., SAHU N., 2008, *Visible light induced photocatalytic activity of rare earth titania nanocomposite.* J Mol Catal A Chem 287, 151-158.

PFALARAS P., LE GOFF A.H., BERNARD M.C., XAGAS A., 2000, *Characterization by resonance Raman spectroscopy of sol–gel TiO₂ films sensitized by the Ru(PPh3)(2)(dcbipy)Cl-2 complex for sol.* Solar Energy Mater Solar Cells, 64, 167-184.

QINGHONG Z., LIAN. G., JINGKUN G., 2000, *Effects of calcination on the photocatalytic properties of nanosized TiO₂ powders prepared by TiCl₄ hydrolysis.* Appl Catal B Environ, 26, 207-215.

RESZCZYNSKA J., GRZYB T., SOBCZAK J.W., LISOWSKI W., GAZDA M., OHTANI B., ZALESKA A., 2015, *Visible light activity of rare earth metal doped (Er³⁺, Yb³⁺or Er³⁺/Yb³⁺) titania photocatalysts.* Appl Catal B Environ, 163, 40-49.

SORAA B., ANA M.B.D.R., LUIS F.V.F., 2010, *Photocatalytic activity of Li⁺ –Rb⁺ –Y³⁺ doped or codoped TiO₂ under sunlight irradiation.* Mater Res Bull, 45, 818-825.

STENGL V., BAKARADJIEVA S., MURAFA N., 2009, *Preparation and photocatalytic activity of rare earth doped TiO₂ nanoparticles.* Mater Chem Phys, 114, 217-226.

STENGL V., KRALOVA P.D., 2011, *Photoactivity of brookite–rutile TiO₂ nanocrystalline mixtures obtained by heat treatment of hydrothermally prepared brookite.* Mater Chem Phys, 129, 794-801.

SUMSMITA P., PAWAN C., AMARJYOTI C., 2014, *Effect of manganese doping on the optical property and photocatalytic activity of nanocrystalline titania: Experimental and theoretical investigation.* J Alloys Comp, 583, 578-586.

VISWANATHAN B., KRISHANMURTHY K.R., 2012, *Nitrogen incorporation in TiO₂: Does it make a visible light photo-active material?* Int J Photoenergy, 10, article ID 269654.

WANG J.L., XU L.J., 2012, *Advanced oxidation processes for wastewater treatment: formation of hydroxyl radical and application.* Crit Rev Environ Sci Technol, 42, 251-325.

XIANGXIN X., WEI J., ZHU M., HUIJUAN M., YUE W., XU W., WEIDONG R., BING Z., JOHN R.L., 2012, *Raman investigation of nanosized TiO$_2$: Effect of crystallite size and quantum confinement.* J Phys Chem C, 116, 8792-8797.

XIE Y., YUAN C., 2003, *Visible-light responsive cerium ion modified titania sol and nanocrystallites for X-3B dye photodegradation.* Appl Catal B Environ, 46, 251-259.

YUAN S., SHENG Q., ZHANG J., CHEN F., ANPO M., ZHANG Q., 2005, *Synthesis of La^{3+} doped mesoporous titania with highly crystallized walls.* Micropor Mesopor Mater, 79, 93-99.

ZHENG S., JIANG W., CAI Y., DIONYSIOU D.D., O'SHEA K.E., 2014, *Adsorption and photocatalytic degradation of aromatic organoarsenic compounds in TiO$_2$ suspension.* Catal Today, 224, 83-88.

ZHU J.F., ZHANG J.L., CHEN F., IINO K., ANPO M., 2005, *High activity TiO$_2$ photocatalysts prepared by a modified sol–gel method: Characterization and their photocatalytic activity for the degradation of XRG and X-GL.* Top Catal, 35, 261-268.